POLITECNICO DI TORINO
Repository ISTITUZIONALE

Curl-Constrained Gradient Estimation for Image Recovery from Highly Incomplete Spectral Data

Original
Curl-Constrained Gradient Estimation for Image Recovery from Highly Incomplete Spectral Data / Ravazzi, Chiara; Coluccia, Giulio; Magli, Enrico. - In: IEEE TRANSACTIONS ON IMAGE PROCESSING. - ISSN 1057-7149. - STAMPA. - 26:6(2017), pp. 2656-2668. [10.1109/TIP.2017.2685342]

Availability:
This version is available at: 11583/2671646 since: 2021-03-16T16:06:33Z

Publisher:
Institute of Electrical and Electronics Engineers Inc.

Published
DOI:10.1109/TIP.2017.2685342

Terms of use:

This article is made available under terms and conditions as specified in the corresponding bibliographic description in the repository

Publisher copyright
IEEE postprint/Author's Accepted Manuscript

©2017 IEEE. Personal use of this material is permitted. Permission from IEEE must be obtained for all other uses, in any current or future media, including reprinting/republishing this material for advertising or promotional purposes, creating new collecting works, for resale or lists, or reuse of any copyrighted component of this work in other works.

(Article begins on next page)

20 April 2024

Curl-constrained Gradient Estimation for Image Recovery from Highly Incomplete Spectral Data

Chiara Ravazzi, *Member, IEEE*, Giulio Coluccia, *Member, IEEE*, and Enrico Magli, *Fellow, IEEE*

***Abstract*—In this paper, we introduce new gradient-based methods for image recovery from a small collection of spectral coefficients of the Fourier transform, which is of particular interest for several scanning technologies, such as magnetic resonance imaging.**

Since gradients of a medical image are much more sparse or compressible than the corresponding image, classical ℓ_1-minimization methods have been used to recover these relative differences. The image values can then be obtained by integration algorithms imposing boundary constraints.

Compared to classical gradient recovery methods, we propose two new techniques that improve reconstruction. First, we cast the gradient recovery problem as a compressed sensing problem taking into account that the curl of the gradient field should be zero. Second, inspired by the emerging field of signal processing on graphs, we formulate the gradient recovery problem as an inverse problem on graphs. Iteratively reweighted ℓ_1 recovery methods are proposed to recover these relative differences and the structure of the similarity graph. Once the gradient field is estimated, the image is recovered from the compressed Fourier measurements using least squares estimation.

Numerical experiments shows that the proposed approach outperforms the state-of-the-art image recovery methods.

***Keywords*—Compressed sensing, Fourier transform, Sparse recovery, Spectral graph theory, Total variation.**

I. Introduction

The recovery of an image from Fourier measurements plays a very important role in several scanning technologies, such as magnetic resonance imaging (MRI, [1]) and synthetic aperture radar [2]. In this context, one would like to reduce the scan time and acquire the smallest number of measurements allowing recovery with the highest quality.

Compressed sensing [3] has emerged in the last few years as a valuable approach to reduce the amount of spectral data needed for reconstruction. Indeed, CS has been shown to effectively recover signals from a limited number of samples by taking advantage of the sparse nature of such signals in a certain domain. The method can be extended to several scenarios and higher dimensions. For example, it can be shown that, under certain conditions on the number of measurements, a piecewise constant image can be recovered from incomplete frequency samples by minimizing total variation (TV, [4]). Given these encouraging results, much effort has been spent in literature to design solvers for TV minimization (such as as ℓ_1-magic [5], TwIST [6], [7], NESTA [8], [9], TVAL3 [10], [11], RecPF [12] and so on).

Although TV minimization allows a significant reduction in the number of measurements needed for reconstruction, reconstructed images often suffer from undesirable artifacts and image details tend to be over-smoothed. Moreover, this method does not fully exploit the sparsity in the gradient of an image. In [13], starting from the observation that Fourier coefficients of the gradient can be obtained from the diagonal transformation of the Fourier transform of the original image, a new algorithm for image reconstruction, labelled as GradientRec–Diff, has been proposed. In a nutshell, given the set of spectral data, the horizontal and vertical differences are retrieved from compressed measurements; the image is then recovered using an integration method. As shown in [13], GradientRec–Diff shows better performance than RecPF, at the price of higher complexity, for low undersampling regimes. However, when the number of measurements is very small, RecPF achieves better reconstruction error.

To overcome these drawbacks, in this paper we propose a new gradient based method for image recovery. In particular, we propose two new strategies for gradient recovery, namely, Curl-constrained Gradient Estimation (CCGE) and iteratively reweighted ℓ_1-CCGE. In the first approach, we cast the gradient recovery problem as a compressed sensing problem enforcing both the sparsity and the directional continuity in the image gradient domain. Indeed, given incomplete information or presence of noise, the reconstructed gradient field by GradientRec–Diff might be not conservative and, consequently, non-integrable. In the proposed method we enforce that the integral along any closed curve should be equal to zero, as it allows to obtain a more accurate estimation of the image gradient and, consequently, a better image reconstruction quality, as we will show in the following sections. In the second method, inspired by the emerging field of signal processing on graphs, the gradient recovery problem is formulated as an inverse problem on graphs. More precisely, a graph is defined on the data units of the image: each unit is associated to a graph node and an edge is drawn according to the similarity between the image values. Iteratively reweighted ℓ_1 recovery methods are proposed to retrieve the relative differences and to infer the structure of the similarity graph. Once the gradient field is estimated, the image is recovered using least squares estimation.

Chiara Ravazzi is with the National Research Council (CNR), Institute of Electronics, Computer and Telecommunication Engineering (IEIIT), c/o Politecnico di Torino, Torino, Italy. E-mail: chiara.ravazzi@ieiit.cnr.it.

Giulio Coluccia is with the Dept. of Electronics and Telecommunications, Politecnico di Torino, Torino, Italy. E-mail: giulio.coluccia@polito.it.

Enrico Magli is with the Dept. of Electronics and Telecommunications, Politecnico di Torino, Torino, Italy, and is also Research Associate with CNR-IEIIT, Torino, Italy. E-mail: enrico.magli@polito.it.

This work was supported by the European Research Council under the European Communitys Seventh Framework Programme (FP7/2007-2013)/ERC Grant agreement n. 279848.

Numerical experiments show that the proposed approach outperforms the state-of-the-art image recovery methods in terms of relative error in several scenarios. More precisely, in absence of noise the proposed CCGE algorithms achieve perfect reconstruction with the lowest number of samples. We show that they are also robust against noise, outperforming classical TV minimization for sparse recovery in terms of accuracy for high signal-to-noise ratios. Finally, tests on real MRI images show improved reconstruction for several sampling patterns.

A. Outline of the paper

The paper is organized as follows. The general image recovery problem from incomplete Fourier measurements and classical algorithms based on CS are introduced in Section II. In Section III the proposed algorithms for gradient estimation are presented and the relations to the state of the art are discussed. Section III-B describes the proposed image reconstruction method from the estimated gradient field. Section IV collects several numerical experiments and some concluding remarks (Section V) complete the paper. We conclude this section with some notations and preliminary definitions.

B. General notation

Throughout this paper, we use the following notation. Let $\mathbb{N}, \mathbb{R}, \mathbb{C}$ be the set of natural, real, and complex numbers, respectively. Given $N \in \mathbb{N}$, we define the set of integers $[N] = \{0, 1, \dots, N-1\}$. The imaginary part of the unit is denoted by $\mathrm{j} = \sqrt{-1}$.

We denote column vectors with small letters, and matrices with capital letters. Given a matrix $X \in \mathbb{R}^{m\times n}$, each entry is denoted with $X_{i,\ell}$ or $X(i,\ell)$, depending on the convenience. $X^\top$ denotes its transpose, X^{H} its hermitian and $X^\dagger$ its Moore-Penrose pseudo-inverse. X^+ is the matrix whose entries are $X^+_{i,\ell} = 1/X_{i,\ell}$ with the convention that $1/0 = 0$. $x = \mathrm{vec}(X)$ denotes the column vector obtained by stacking the columns of X on top of each other, while $X = \mathrm{vec}^{-1}(x)$ denotes the inverse operation. $A = \mathrm{diag}(a)$ denotes the square diagonal matrix with a on its diagonal. The elementwise product of matrices A and B is denoted by $A \odot B$. The Kronecker product of matrices A and B is denoted by $A \otimes B$. Let $\nabla X = (\nabla_x X, \nabla_y X) \in \mathbb{R}^{m\times n\times 2}$ be the discrete gradient operator:

$$(\nabla_x X)_{i,\ell} = X_{i,\ell} - X_{i-1,\ell}$$
$$(\nabla_y X)_{i,\ell} = X_{i,\ell} - X_{i,\ell-1}.$$

Given a vector field (F_1, F_2) the curl is defined as

$$\mathrm{curl}(F_1, F_2) = \nabla_y F_1 - \nabla_x F_2.$$

The discrete TV operator and the TV semi-norm of X are defined as follows

$$(\mathrm{TV}(X))_{i,\ell} = \sqrt{|(\nabla_x X)_{i,\ell}|^2 + |(\nabla_y X)_{i,\ell}|^2}$$
$$\|X\|_{\mathrm{TV}} = \|\mathrm{TV}(X))\|_1,$$

where

$$\|X\|_p = \left(\sum_{i=1}^{m}\sum_{j=1}^{m} |X_{i,\ell}|^p\right)^{1/p}$$

and

$$\|X\|_0 = \sum_{i=1}^{m}\sum_{j=1}^{m} |X_{i,\ell}|^0$$

with the convention that $0^0 = 0$. We say that X is k-sparse in the gradient domain if $\|\nabla X\|_0 = k$.

A directed graph is a pair $\mathcal{G} = (\mathcal{V}, \mathcal{E})$, where $\mathcal{V}$ is the set of nodes and $\mathcal{E} \subseteq \mathcal{V} \times \mathcal{V}$ is the set of edges. We say that $\mathcal{G} = (\mathcal{V}, \mathcal{E})$ is an undirected graph if $(u, v) \in \mathcal{E}$ implies that (v, u) is also an edge in $\mathcal{E}$. A path in a graph is a sequence of edges which connects a sequence of vertices. In a directed graph $\mathcal{G}$, two vertices u and v are called connected if there exists a path from u to v. A graph is said to be connected if every pair of vertices in the graph is connected. A directed graph $\mathcal{G}$ is called strongly connected if there is a path from each vertex in the graph to every other vertex.

II. Image recovery from spectral data

Let $F \in \mathbb{R}^{m\times n}$ be an image and denote $N = mn$. Each pixel of the image can be identified by a pair of indexes $(u_x, u_y) \in [m] \times [n]$ corresponding to the row and to the column. Let $\mathcal{F} : \mathbb{R}^{m\times n} \to \mathbb{C}^{m\times n}$ be the bidimensional DFT of F:

$$[\mathcal{F}(F)]_{\underline{\omega}} = \frac{1}{\sqrt{N}} \sum_{u_x\in[m]} \sum_{u_y\in[n]} F(u_x, u_y) \mathrm{e}^{-2\pi \mathrm{j}(\omega_x u_x/n + \omega_y u_y/m)}.$$

Defined a set of $M << N$ frequencies

$$\Omega = \{\underline{\omega}^{(k)} = (\omega_x^{(k)}, \omega_y^{(k)}) : k \in \{1, \dots, M\}\},$$

our aim is to recover the image F from partial frequency information $[\mathcal{F}(F)]_\Omega$, affected by bounded noise. More precisely, we are interested in image recovery starting from partial observations of the form

$$y = \mathcal{F}_\Omega(F) + \eta \tag{1}$$

with $\|\eta\|_2 = \epsilon$.

Since CS has been shown to effectively recover signals from a limited number of samples by taking advantage of the sparse nature of such signals in a certain domain, this approach has been extended to the reconstruction of approximately piecewise constant images [4]. The literature proposes a huge number of solvers based on this intuition. We distinguish two categories: Image recovery based on total variation minimization and Gradient-based image recovery. We summarize these approaches in the remaining section.

A. Total variation minimization

Classical CS recovery solves this problem assuming that natural images are sparse in a certain domain, such as DCT, wavelets, shearlets, and so on. Particular attention has been devoted to TV recovery methods [4], [1], [3]. They explore the prior knowledge that medical images are sparse in the gradient domain [4]. More precisely, TV problem is defined as follows:

$$\widehat{F}_{\text{TV}} = \underset{X\in\mathbb{R}^{m\times n}}{\arg\min} \|X\|_{\text{TV}} \qquad \text{s.t. } \|\mathcal{F}_\Omega(X) - y\|_2 \leq \epsilon. \tag{2}$$

In absence of noise (i.e. $\epsilon = 0$ in (1)) and if the image is piecewise constant, theoretical guarantees for perfect reconstruction are proven (see [4, Theorem 1.5]). More precisely, if F is a k-sparse image in the gradient domain and Ω is chosen uniformly at random with $M = O(k\log^4 N)$, then the solution to (2) is unique and is equal to F with probability larger than $1 - O(N^{-M})$.

Several algorithms have been proposed in literature to solve (2), as ℓ_1-magic [5], TwIST [6], [7], NESTA [8], [9], and TVAL3 [10], [11], to mention just a few. Among them, TVAL3 is faster compared to the other TV solvers. A new algorithm for reconstruction of images from partial Fourier measurements, known as RecPF, has been proposed in [12]. This method, based on a fast alternating direction method, achieves the best CS recovery results, outperforming TwIST and OS [14]. It attempts to solve the following relaxed problem

$$\min \frac{1}{2}\|\mathcal{F}_\Omega(F) - y\|^2 + \gamma\|\Psi F\|_1 + \lambda\|F\|_{\text{TV}}, \tag{3}$$

where λ and γ are regularization parameters and Ψ a sparsifying basis.

B. Gradient-based image recovery

Despite high CS effectiveness in image reconstruction, TV minimization based methods do not exploit the sparsity that is revealed in the gradient of an image. Indeed, as shown in [13], the absolute magnitude of the gradients, both in the horizontal and vertical directions, decay much faster than the TV coefficients.

Starting from this observation, in [13] a different approach to the recovery problem is proposed. Given the set of Fourier measurements of an image, the following steps are performed: i) a diagonal transformation to obtain the Fourier measurements of the horizontal and vertical gradients, ii) a gradient estimation from incomplete Fourier measurements, and iii) an image reconstruction from estimated gradient field. The steps of this procedure, called GradientRec–Diff, are described in detail as follows.

1) Diagonal transformation: Simple computations show that the Fourier measurements of $\nabla_x F$ and $\nabla_y F$ can be obtained by a diagonal transformation of the Fourier transform of the original image. More specifically,

$$[\mathcal{F}(\nabla_x F)]_{\underline{\omega}} = (1 - \mathrm{e}^{-2\pi\mathrm{j}\omega_x/N})[\mathcal{F}_\Omega(F)]_{\underline{\omega}} \tag{4}$$

$$[\mathcal{F}(\nabla_y F)]_{\underline{\omega}} = (1 - \mathrm{e}^{-2\pi\mathrm{j}\omega_y/N})[\mathcal{F}_\Omega(F)]_{\underline{\omega}} \tag{5}$$

where $\underline{\omega} \in \Omega$.

Taking into account the presence of noise in model (1) we consider the following observations

$$y_x = \Lambda_x y = \mathcal{F}_\Omega(\nabla_x F) + \eta_x \tag{6}$$

$$y_x = \Lambda_x y = \mathcal{F}_\Omega(\nabla_y F) + \eta_y \tag{7}$$

where

$$\Lambda_x = \text{diag}(1 - \mathrm{e}^{-2\pi\mathrm{j}\omega_x/N}) \tag{8}$$

$$\Lambda_y = \text{diag}(1 - \mathrm{e}^{-2\pi\mathrm{j}\omega_y/N}), \tag{9}$$

and $\|\eta_x\|_2 = \|\Lambda_x\eta\|_2 = \epsilon_x$, $\|\eta_y\|_2 = \|\Lambda_y\eta\|_2 = \epsilon_y$.

2) Gradient estimation: Once the Fourier measurements of the gradients are computed, $\nabla_x F$ and $\nabla_y F$ are estimated exploiting sparsity and using convex optimization methods:

$$\widehat{G}_x = \underset{G_x\in\mathbb{R}^{m\times n}}{\arg\min} \|G_x\|_1 \quad \text{s.t.} \quad \|\mathcal{F}_\Omega(G_x) - y_x\|_2 \leq \epsilon_x \tag{10}$$

$$\widehat{G}_y = \underset{G_y\in\mathbb{R}^{m\times n}}{\arg\min} \|G_y\|_1 \quad \text{s.t.} \quad \|\mathcal{F}_\Omega(G_y) - y_y\|_2 \leq \epsilon_x \tag{11}$$

The advantage of this method is that the gradients of the image can be computed independently. Moreover, different CS recovery algorithms can be used for edge reconstruction, such as OMP [15], CoSaMP [16], ℓ_p-minimization methods with $p < 1$ [17], iteratively reweighted ℓ_1-minimization algorithms [18].

3) Image reconstruction: Once approximations to the horizontal and vertical gradient are obtained, the image should be recovered using an integration method. However, given the incomplete information or the presence of noise, the estimated gradient field might be not conservative making it non-integrable. Indeed, if the integral along any closed curve is not equal to zero, the reconstruction method should depend on the path of integration. Several methods have been proposed in literature to enforce the integrability [13], [19].

We discuss here the integration method based on affine transformation using diffusion tensor [20]. The performance of this method does not depend on the type of sampling and enforces integrability using the information contained in the curl of non-integrable estimated gradient field. More precisely, using a Least Squares (LS) approach for image reconstruction requires to solve the following minimization problem:

$$\begin{aligned} &\min_{X\in\mathbb{R}^{m\times n}} \|\nabla_x X - \widehat{G}_x\|_2^2 + \|\nabla_y X - \widehat{G}_y\|_2^2 \\ &\text{s.t. curl}(\nabla_x X, \nabla_y X) = 0 \end{aligned} \tag{12}$$

When $\text{curl}(\widehat{G}_x, \widehat{G}_y)$ is non-zero, the problem yields a linear system that is under-determined, with more unknowns than the number of equations. To overcome this issue, the number of unknowns is reduced assuming that the gradient values with lowest curl are error free. Then, imposing Neumann boundary conditions, the solution is unique.

III. Proposed approach

In this section we propose a new method for image recovery. We aim at reducing as much as possible the number of measurements required for a satisfactory recovery. We propose several solutions to this problem. Our approach falls under

Diagonal transformation
↓
Gradient estimation
↓
Image reconstruction.

the second category, i.e. gradient based methods for image recovery, since it follows the same flow of reconstruction:

In the Diagonal transformation step, the measurements of the gradient are obtained as explained in point 1) of Section II.B. The differences with respect to GradientRec–Diff lie in the Gradient estimation step and in Image reconstruction step. We explain the rationale in the following.

A. Gradient estimation

We propose now two methods for Gradient estimation. The first approach is based on the observation that the gradient is overdetermined gradient and its estimation can not be contraint-free. In the second method, using the same observation, we formulate the image recovery problem as a constrained inverse problem on graphs and propose an iteratively reweighted ℓ_1 recovery algorithm to recover the gradient and the structure of the similarity graph.

1) Curl-constrained gradient estimation (CCGE): When the number of measurements is very small, the gradient estimation obtained via BP or BPDN (10), (11) is affected by errors. Consequently, the estimated gradient field is necessarily not conservative and these errors are not spread uniformly throughout the gradient field but concentrated around the edges of the image. As a consequence, these errors affect also the image recovery.

Our algorithm is based on the following observation. The gradient of an image $F \in \mathbb{R}^{m\times n}$ is described by $2mn$ pixels. In this sense, the gradient is over-determined and the values of the gradient must be constrained. It should be verified that the gradient of an image is a conservative vector field and satisfies

$$\mathrm{curl}(\nabla_x F, \nabla_y F) = \nabla_y \nabla_x F - \nabla_x \nabla_y F = 0.$$

In the light of the above observation, besides (6) and (7), we take into account that the curl of the reconstructed gradient field should be zero.

In absence of noise, denoted the unknown gradient of an image (G_x, G_y) this fact yields the solution of the following optimization problem:

$$\underset{G_x,G_y\in\mathbb{R}^{m\times n}}{\arg\min} \|G_x\|_1 + \|G_y\|_1 \quad \text{s.t.} \begin{cases} \mathcal{F}_\Omega(G_x) = y_x \\ \mathcal{F}_\Omega(G_y) = y_y \\ \mathrm{curl}(G_x, G_y) = 0 \end{cases}, \quad (13)$$

or, in case of noisy measurements,

$$\underset{G_x,G_y\in\mathbb{R}^{m\times n}}{\arg\min} \|G_x\|_1 + \|G_y\|_1 \quad \text{s.t.} \left\| \begin{bmatrix} y_x \\ y_y \end{bmatrix} - \begin{bmatrix} \mathcal{F}_\Omega(G_x) \\ \mathcal{F}_\Omega(G_y) \end{bmatrix} \right\|^2 + \|\mathrm{curl}(G_x, G_y)\|^2 \le \epsilon_x^2 + \epsilon_y^2 \ . \quad (14)$$

In our experiments we will use a modified version of algorithms SPGL1 [21], [22] and CoSaMP [16] to solve (13) and (14), taking into account the additional constraint on the curl. It should be mentioned that other CS recovery algorithms with the additional constraint on the curl can be used for edge reconstruction, such as OMP [15].

2) Iteratively reweighted ℓ_1-CCGE with Gaussian weights: We now formulate the image recovery problem using graph theory. Let $F \in \mathbb{R}^{m\times n}$ be an image with $N = mn$. Each pixel of the image is labeled with a vertex $u \in \mathcal{V}$ and can be identified by a pair of indexes $(u_x, u_y) \in [m] \times [n]$ corresponding to the row and to the column. We consider the signal f, defined on the set of vertices $f : \mathcal{V} \to \mathbb{R}$ with the vector $f \in \mathbb{R}^N$, where the u-th entry represents the image value at the vertex $f_u = F(u_x, u_y)$.

The gradients are represented as the edges $\mathcal{E} \subseteq \mathcal{V} \times \mathcal{V}$ of an oriented graph $\mathcal{G} = (\mathcal{V}, \mathcal{E})$. Each node u belonging to the interior of the image (*i.e.*, not on its boundary) has four edges, connecting it to nodes in north, south, east, and west directions. Therefore, the resulting graph is a grid. The orientation of the edge e connecting nodes u and v is conventionally assumed (u, v) with $u < v$. The graph topology is encoded in the incidence matrix $A \in \{0, \pm 1\}^{\mathcal{E}\times\mathcal{V}}$ defined by

$$A_{ew} = \begin{cases} +1 & \text{if } e \text{ enters vertex } w \\ -1 & \text{if } e \text{ leaves vertex } w \\ 0 & \text{if } w \text{ is not a vertex of } e \end{cases} \quad (15)$$

for every $e \in \mathcal{E}$ and $w \in \mathcal{V}$. We denote

$$g = \begin{bmatrix} g_x \\ g_y \end{bmatrix} = \begin{bmatrix} A_x \\ A_y \end{bmatrix} f = Af$$

where A_x and A_y are the incidence matrices corresponding to the horizontal and vertical directions, respectively, and $g_x = \mathrm{vec}(\nabla_x F)$ and $g_y = \mathrm{vec}(\nabla_y F)$. In absence of noise, the CCGE problem in (13) becomes

$$\underset{g_x,g_y\in\mathbb{R}^{mn}}{\arg\min} \|g_x\|_1 + \|g_y\|_1 \quad \text{s.t.} \begin{cases} y_x = \mathcal{F}_\Omega(g_x) \\ y_y = \mathcal{F}_\Omega(g_y) \\ A_y g_x - A_x g_y = 0 \end{cases}, \quad (16)$$

or, in presence of noise,

$$\underset{g_x,g_y\in\mathbb{R}^{m\times n}}{\arg\min} \|g_x\|_1 + \|g_y\|_1 \quad \text{s.t.} \left\| \begin{bmatrix} y_x \\ y_y \end{bmatrix} - \begin{bmatrix} \mathcal{F}_\Omega(g_x) \\ \mathcal{F}_\Omega(g_y) \end{bmatrix} \right\|^2 + \|A_y g_x - A_x g_y\|^2 \le \epsilon_x^2 + \epsilon_y^2 \ . \quad (17)$$

In the following paragraph we introduce a new iterative reweighted ℓ_1 method based on weighting according to the similarity among pixels.

In order to obtain high quality CS reconstruction, we modify the CCGE problem using both local smoothness and nonlocal self-similarity. Starting from an initial guess of the gradient, the idea is to use the current estimation of the gradient in order to detect the elements that are most likely to be in the

gradient support. Then, a better estimation of the signal is obtained solving the optimization problem by replacing the ℓ_1-norm with the weighted one in order to avoid penalizing the elements that are most likely to be nonzero. More precisely, we consider the following weighted ℓ_1-problem

$$\begin{aligned}\underset{g_x,g_y\in\mathbb{R}^{\mathcal{V}}}{\arg\min}\sum_{i\in\mathcal{V}} w\left([g_x]_i\right)|[g_x]_i| + w\left([g_y]_i\right)|[g_y]_i| \\ \text{s.t.}\ \begin{cases} y_x = \mathcal{F}_\Omega(g_x) \\ y_y = \mathcal{F}_\Omega(g_y) \\ A_y g_x - A_x g_y = 0 \end{cases},\end{aligned} \tag{18}$$

where

$$w(x) = \mathrm{e}^{-\frac{x^2}{2\theta^2}}$$

is the Gaussian kernel weighting function. The weight function is defined in such a way $w(x) \in (0,1]$ is decreasing in x and is vanishing to zero if $x \to \infty$. On the other side, if $x \to 0$ then $w(x) \to 1$. This choice of weights has been shown effective in graph signal processing to capture the geometric structure of the underlying images, to compress and to denoise images [23].

It should be noted that this non-convex optimization problem is quite difficult to solve directly due to the non-differentiability and non-linearity. In this section, the iteratively reweighted ℓ_1-CCGE algorithm is developed to solve (18). We initialize $g_x^{(0)} = g_y^{(0)} = 0$, then at each iteration $t \in \mathbb{N}$ we compute

$$\begin{aligned} w_x^{(t)} &= \mathrm{e}^{-\frac{\left(g_x^{(t)}\right)^2}{2\theta^2}}, \quad w_y^{(t)} = \mathrm{e}^{-\frac{\left(g_y^{(t)}\right)^2}{2\theta^2}} \\ g^{(t+1)} &= \underset{g_x,g_y\in\mathbb{R}^{\mathcal{V}}}{\arg\min}\sum_{i\in\mathcal{V}} w_x^{(t)}|[g_x]_i| + w_y^{(t)}|[g_y]_i| \\ &\text{s.t.}\ \begin{cases} y_x = \mathcal{F}_\Omega(g_x) \\ y_y = \mathcal{F}_\Omega(g_y) \\ A_y g_x - A_x g_y = 0 \end{cases}. \end{aligned} \tag{19}$$

In our experiments we will use a modified version of algorithm IRL1 [18] to solve (18), taking into account the additional constraint on the curl and the weights update in (19). It should be mentioned that other CS recovery algorithms with the additional constraint on the curl can be used for edge reconstruction, such as OMP [15].

B. Image reconstruction

We let $\widehat{g} \in \mathbb{R}^{\mathcal{E}}$ be the vector collecting the estimated gradient field and denote

$$\widehat{g} = Af + \xi,$$

where ξ is the error obtained on the gradient estimation.

Assuming that the error ξ is distributed as Gaussian noise, we take a least-squares approach for estimating the signal f starting from measurements $\widehat{g}$. That is, we define the following unconstrained quadratic optimization problem

$$\min_{x\in\mathbb{R}^N} \frac{1}{2}\|Ax - \widehat{g}\|_2^2. \tag{20}$$

It should be noticed that, being $A\mathbb{1} = 0$, the solution is not unique. The set of solutions of (20) is described in the following well-known lemma [24].

Lemma 1 (LS estimator)**.** *Let the graph $\mathcal{G}$ be connected and let $L_{\mathcal{G}} := A^\top A$ denote the Laplacian of the graph. The following facts hold:*

1) *x is a solution to* (20) *if and only if $A^\top Ax = A^\top \widehat{g}$;*
2) *there exists a unique minimizer of* (20) *$\widehat{x}^{\mathrm{ls}}$ with minimum $\|\widehat{x}^{\mathrm{ls}}\|_2$;*
3) *$\widehat{f}^{\mathrm{ls}} = L_{\mathcal{G}}^\dagger A^\top \widehat{g}$.*

Further useful properties are the following.

Proposition 1 (Moments of LS estimator)**.** *For the LS estimator, it holds true that*

$$\begin{aligned}\mathbb{E}[\widehat{f}^{\mathrm{ls}}] &= \big(I - \frac{1}{N}\mathbb{1}\mathbb{1}^\top\big) f \\ \mathbb{E}[(\widehat{f}^{\mathrm{ls}} - \mathbb{E}[f^{\mathrm{ls}}])(\widehat{f}^{\mathrm{ls}} - \mathbb{E}[\widehat{f}^{\mathrm{ls}}])^{\mathsf{H}}] &= L_{\mathcal{G}}^\dagger\end{aligned}$$

It should be noted that determining the signal $\widetilde{f}$ from relative measurements is only possible up to an additive constant. This ambiguity can be avoided by taking

$$\widetilde{f} = \widehat{f}^{\mathrm{ls}} + \frac{1}{N}\mathbb{1}\mathbb{1}^\top f$$

Moreover, if $0 \in \Omega$ the second term is equal to $y(0)/\sqrt{N}$ leading to

$$\widetilde{f} = \widehat{f}^{\mathrm{ls}} + \frac{y(0)}{\sqrt{N}}\mathbb{1}.$$

These preliminary results yield the following theorem, whose proof can be easily obtained.

Theorem 1. *Let $\widehat{g} \in \mathbb{R}^{\mathcal{E}}$ be the estimated gradient field and assume that $0 \in \Omega$, U eigenvectors of the Laplacian of the square grid, and D the diagonal matrix of corresponding eigenvalues. Then*

$$\widetilde{f} = UD^\dagger U^\top A^\top \widehat{g} + \frac{y(0)}{\sqrt{N}}.$$

The $N = mn$ eigenvalues of the Laplacian of the square grid graph (contained in the diagonal of D) and the corresponding eigenvectors (collected as columns of U) can be evaluated according to the following lemma

Lemma 2. *The eigenvalues of the Laplacian of the square grid graph are*

$$4\sin^2\left(\frac{\pi s}{2m}\right) + 4\sin^2\left(\frac{\pi l}{2n}\right), \tag{21}$$

with $s \in [m]$ and $\ell \in [n]$. The corresponding eigenvectors are

$$u^s \otimes u^\ell$$

where

$$\begin{aligned} u^s(i) &= \cos\left(\frac{\pi\ell}{m}\,(i+1/2)\right) \\ u^\ell(i) &= \cos\left(\frac{\pi\ell}{n}\,(i+1/2)\right) \end{aligned}$$

It should be noticed that the eigenvectors of this matrix are exactly the DCT Type II basis vectors (see [25]). Hence, the procedure to recover the image from the estimated gradient field can be efficiently implemented via the bidimensional DCT: given $\widehat{g}$, first $A^\top \widehat{g}$ is resized to match the size of the image; then the direct and inverse DCT are performed as stated in the following corollary.

Corollary 1. *Let $\widehat{g} \in \mathbb{R}^{\mathcal{E}}$ be the estimated gradient field and assume that $0 \in \Omega$, Λ the eigenvalues of the Laplacian of the square grid. Then*

$$\widetilde{f} = \mathrm{IDCT}_2\left[(\Lambda^+) \odot \mathrm{DCT}_2\left[\mathrm{vec}^{-1}(A^\top \widehat{g})\right]\right] + \frac{y(0)}{\sqrt{N}} \ , \quad (22)$$

where $\Lambda_{s,\ell}$ is given in (21).

IV. Numerical results

In this section we test the following algorithms:

- $\diamond$ ℓ_1-CCGE–LS (*i.e.*, the algorithm recovering the gradient of the image as in Section III-A2 and reconstructing the image using (22));
- $\diamond$ CoSaMP-CCGE–LS (*i.e.*, the algorithm recovering the gradient of the image solving (13) using CoSaMP and reconstructing the image using (22));
- $\diamond$ GradientRec–Diff [13], described in detail in Section II-B, which first separately estimates the gradient on rows and the gradient on columns, then reconstructs the image from its gradient using an integration method based on diffusion tensors [26];
- $\diamond$ RecPF [12], a fast and efficient method for the minimization of the Total Variation of the reconstruction from incomplete Fourier measurements (3).

We report, as benchmark, the reconstruction results of an *Oracle* device, whose behavior is similar to the ℓ_1-CCGE–LS algorithm, with the difference that the Oracle reconstructs in a single step using the optimum weights since it knows perfectly the values of the image gradient. More precisely, it solves (18) with

$$w(\mathrm{vec}(\nabla F)_i) = \mathrm{e}^{-\frac{\mathrm{vec}(\nabla F)_i^2}{2\theta^2}}$$

In this sense, the performance of the Oracle provides the best performance achievable by ℓ_1-CCGE–LS.

We analyze the algorithms under different conditions. In the first set of experiments, described in Section IV-A, we use as test image the 64×64 Shepp–Logan phantom in a noiseless scenario, for different values of the compression ratio $L = M/N$. In the second set of experiments, described in Section IV-B, we fix the compression ratio L and reconstruct the same test image from noisy measurements, for different values of the noise standard deviation σ. In the third set of tests, described in Section IV-C, we test the reconstruction algorithms using actual MRI images. We point out here that all the MRI images used to simulate and compare the proposed algorithms with the state of the art come from real acquisitions made by medical devices on human brains, ankles and knees.

For each set of experiments, three different undersampling patterns, depicted in Figure 1, are used, namely, a radial sampling pattern, a uniformly-distributed sampling pattern and a variable-density sampling pattern. For a thorough analysis of the pros and cons of each sampling pattern, see [3] and [27].

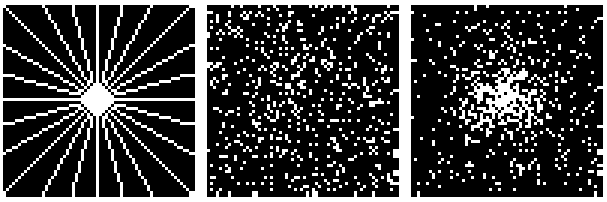

(a) (b) (c)

Fig. 1. 64×64 sampling patterns for given Compression Ratio L. (a) Radial pattern with $L = 0.17$. (b) Uniform pattern with $L = 0.15$. (c) Variable density pattern with $L = 0.15$.

The performance of the algorithms have been evaluated both in term of relative error

$$\frac{\|f - \widetilde{f}\|_2}{\|f\|_2} \ , \quad (23)$$

where $\widetilde{f}$ is the estimated image and f is the true image, and in terms of execution time of the algorithm, in seconds.

For the algorithms requiring the ℓ_1 norm minimization, *i.e.*, the proposed ℓ_1-CCGE–LS and GradientRec–Diff, SPGL1 [21], [22] is used to solve the Basis Pursuit problem in the noiseless case and the Basis Pursuit Denoising in the noisy case. Finally, it has to be remarked that a failure in the reconstruction, *i.e.*, a solver giving a Not-a-Number (NaN) as output, is treated as the algorithm returned a totally black image (all 0s), corresponding to a relative error of 1.

A. Noiseless acquisitions

This section reports the reconstruction results of the 64×64 Shepp–Logan phantom, in a noiseless setting. The compression ratios $L = M/N$ ranges from 0.01 to 0.4. 3 iterations of the ℓ_1-CCGE–LS algorithm have been run, while for RecPF we fixed the parameters γ and λ of (3) to 0 and 10^{-10}, respectively.

Figure 2 shows the results for the radial sampling pattern of Figure 1a. It can be noticed that the proposed CCGE–LS algorithms are the ones showing the best performance, with almost perfect reconstruction for $L \geq 0.17$. RecPF reaches its optimum performance for $L \geq 0.2$ while GradientRec–Diff performs better than RecPF for $L > 0.27$, confirming the behavior obtained in [13]. There is a performance gap between the Oracle and the CCGE–LS.

As for the execution times, the fastest algorithm is RecPF, even if the proposed CoSaMP-CCGE–LS shows really close performance. The ℓ_1-CCGE–LS is the slowest due to the iterative procedure, while GradientRec–Diff has slightly faster performance, especially for high values of L.

Figure 3 visually shows the reconstruction results for $L = 0.17$, as well as the visual representation of the reconstruction error. It can be shown that the reconstruction obtained by the proposed CCGE–LS algorithms are almost perfect, with a relative error of 10^{-7}. RecPF shows an acceptable reconstruction quality (10^{-2}), even if some edge-related artifacts

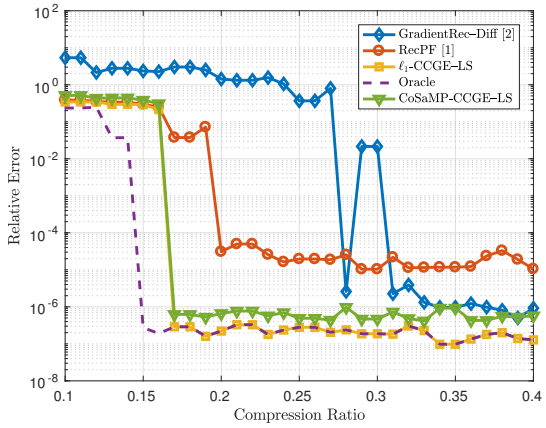

(a)

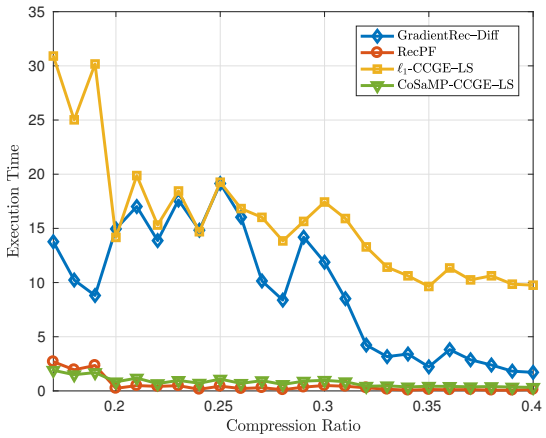

(b)

Fig. 2. Phantom 64×64. Radial sampling. (a) Reconstruction relative error (b) Reconstruction time vs. Compression Ratio.

can be noticed. On the other hand, the reconstruction quality of GradientRec–Diff is significantly worse for $L = 0.17$.

For uniformly distributed sampling pattern (Figure 1b) the results are shown in Figure 4. The results correspond to the average of 50 tests with different realizations of the sampling pattern. Here, it can be noticed that the ℓ_1-CCGE–LS algorithm is the one performing best, with almost-perfect reconstruction for $L \geq 0.14$. As already pointed out, the oracle estimation simply assumes to know the optimal weights in the gradient estimation problem and it clearly represents a performance benchmark to compare against. In Figure 2 (a) and Figure 4 we can appreciate that the gap between the proposed method (ℓ_1-CCGE–LS) and the oracle is very small, suggesting that the proposed method has already achieved the limits of gradient based MRI image recovery.. The CoSaMP-CCGE–LS performs slightly worse, with perfect reconstruction for $L \geq 0.19$, while GradientRec–Diff performs as in the radial sampling case, achieving its best result for $L \geq 0.28$. On the contrary, RecPF seems to suffer the uniformly distributed sampling pattern and could not reconstruct the signal. This will be confirmed in the next sections and is probabily due to the lack of samples corresponding to low frequencies.

Finally, we show in Figure 5 the results for the variable density sampling pattern, depicted in Figure 1c. The results correspond to the average of 50 tests with different realizations of the sampling pattern. Again, the proposed CCGE–LS algorithms are the ones performing best, showing perfect reconstruction for $L \geq 0.15$, even if for $L \geq 0.29$ GradientRec–Diff performs slightly better than CoSaMP-CCGE–LS, while RecPF reaches its best performance for $L \geq 0.17$ even if with a higher error floor. As for the execution times, the same comments given for the radial pattern apply to the random uniform and variable density pattern.

To wrap up, these results show that the proposed CCGE–LS algorithms are the ones with best performance, both in terms of reconstruction error and execution time, and are the least sensitive to the sampling pattern. The additional constraint imposed to the reconstruction of the gradient represents a significant improvement in performance with respect to the GradientRec–Diff algorithm, with a slight loss in terms of execution time, in the case the iterative procedure is adopted (as is in ℓ_1-CCGE–LS). A good compromise is represented by RecPF, which however skips the estimation of the gradient, which may be required for other purposes than image reconstruction, and is highly sensitive to the sampling pattern, requiring it to concentrate the sampling in correspondence of the low frequencies.

B. *Noisy acquisitions*

In this section, we test the performance of the reconstruction from noisy measurements. The undersampled partial Fourier acquisitions are affected by AWGN noise with zero mean and standard deviation σ. For fairness, we test the performance at a compression ratio of $L = 0.4$. Indeed, according to the results of previous section, this value is high enough for all the algorithms to show acceptable quality.

The noise standard deviation σ ranges from 0.01 to 0.1. 5 iterations of the ℓ_1-CCGE–LS algorithm have been run, while for RecPF we fixed the parameters γ and λ of (3) to 0 and σ^2, respectively. The results correspond to the average of 50 tests with different realizations of the noise and the sampling pattern (of the noise only, for radial sampling).

Figure 6 shows the results obtained with radial sampling. It can be noticed that, while GradientRec–Diff shows the worst performance, the proposed CCGE–LS algorithms perform best than RecPF, especially for higher noise variance. When the noise variance is low, RecPF performs slightly better, even if the gap is small with respect to CoSaMP-CCGE–LS.

Figure 7 reports the results obtained with uniformly distributed sampling. In this case, neither RecPF nor GradientRec–Diff are able to reconstruct the signal, while the proposed CCGE–LS algorithms reconstruct the signal with acceptable performance.

Finally, using a variable density sampling pattern, the results are similar to the ones obtained with a radial scheme. Figure 8 reports the obtained performance. While on one hand GradientRec–Diff shows the worst performance, RecPF seems to have slightly better performance than our proposed CCGE–LS for high signal-to-noise ratios. On the other hand, when

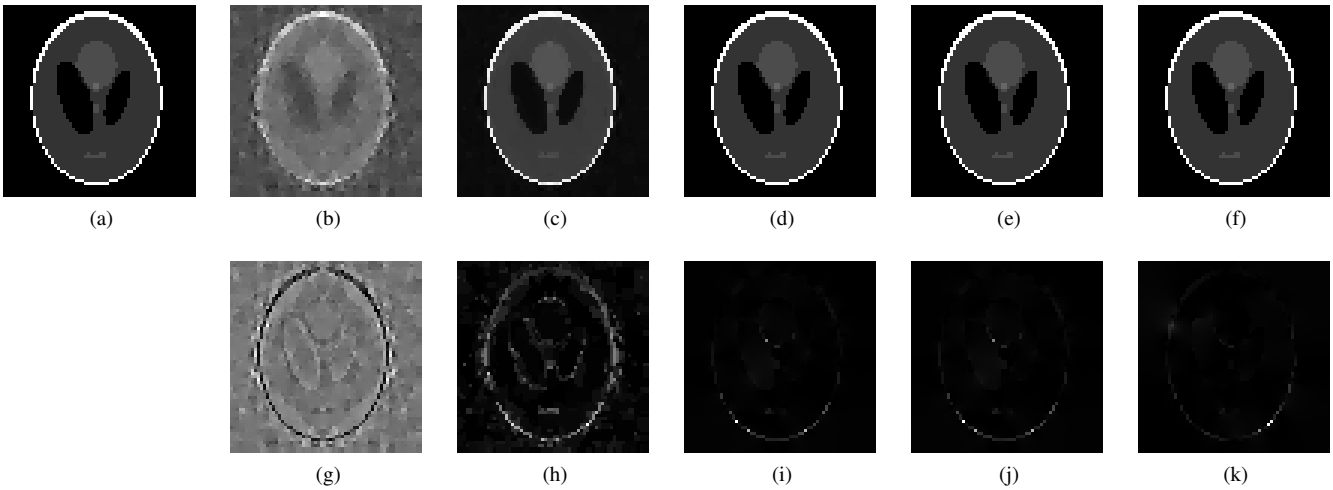

Fig. 3. Phantom 64×64. Radial sampling. Compression Ratio $L = 0.17$. Top line: image reconstruction. Bottom line: error image. (a) Original. (b) and (g) GradientRec–Diff. Relative Error: 3.02. (c) and (h) RecPF. Relative Error: $3.75 \cdot 10^{-2}$. (d) and (i) ℓ_1-CCGE–LS. Relative Error: $2.89 \cdot 10^{-7}$. (e) and (j) Oracle. Relative Error: $2.89 \cdot 10^{-7}$. (f) and (k) CoSaMP-CCGE–LS. Relative Error: $6.24 \cdot 10^{-7}$.

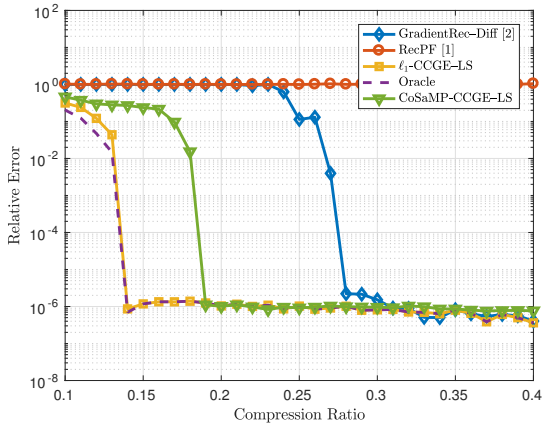

Fig. 4. Phantom 64×64. Uniform sampling. Reconstruction relative error vs. Compression Ratio.

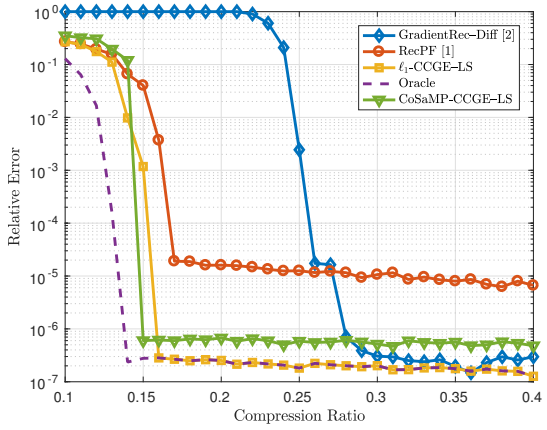

Fig. 5. Phantom 64×64. Variable density sampling. Reconstruction relative error vs. Compression Ratio.

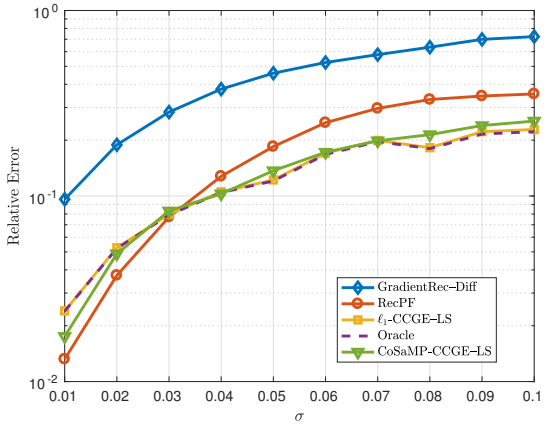

Fig. 6. Phantom 64×64. Radial sampling. Compression ratio $L = 0.4$. Reconstruction relative error vs. noise standard deviation σ.

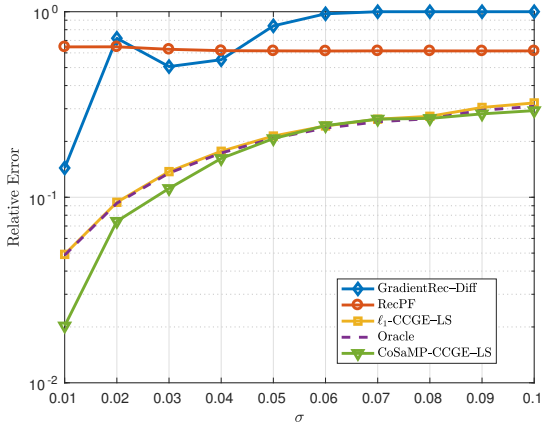

Fig. 7. Phantom 64×64. Uniform sampling. Compression ratio $L = 0.4$. Reconstruction relative error vs. noise standard deviation σ.

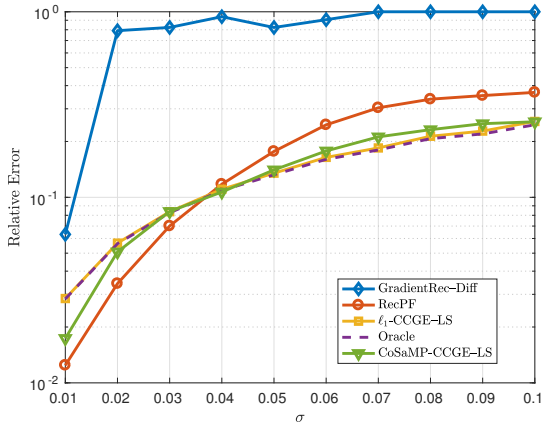

Fig. 8. Phantom 64×64. Variable density sampling. Compression ratio $L = 0.4$. Reconstruction relative error vs. noise standard deviation σ.

$\sigma > 0.03$ the proposed CCGE–LS algorithms perform better than the competing schemes.

For what concerns the execution times, the fastest algorithms are RecPF and GradientRec–Diff with executions times under 1 second. It took between 1 and 10 seconds to ℓ_1-CCGE–LS to complete the reconstruction - with 5 iterations of the algorithm - while it took more than 10 seconds to CoSaMP-CCGE–LS to reconstruct the image.

C. MRI acquisitions

In this section we describe the results obtained from partial Fourier sampling of 512×512 MRI images of a brain, a knee, and an ankle. The Fourier acquisitions of the images have been then undersampled using the radial pattern, the uniformly distributed pattern and the variable density pattern. The compression ratio is set to $L = 0.4$.

Table I reports the reconstruction results in terms of reconstruction relative error (23). A *NaN* denotes a failure in the reconstruction algorithm. Figures 9, 10 and 11 show the reconstruction results for the *Brain* image. Figures 12, 13, and 14 show the reconstruction results for the *Knee* image. Finally, Figures 15, 16, and 17 show the reconstruction results for the *Ankle* image. All the figures show a visual representation of the reconstruction error along with the reconstructed image.

From the results depicted in the figures and summarized in Table I, it can be noticed that

- ◇ the GradientRec–Diff algorithm always performs worse than RecPF and the proposed CCGE–LS algorithm;
- ◇ for the uniformly distributed sampling pattern, the proposed CCGE–LS algorithm is the only reliable algorithm providing satisfactory reconstruction quality;
- ◇ for the *Brain* image, the Total Variation minimization performed by RecPF seems to work better than competing algorithms, except for the uniformly distributed sampling pattern;
- ◇ for the *Knee* image, the proposed algorithm works better than RecPF for the radial and uniformly distributed sampling patterns, but RecPF has slightly better performance for the variable density sampling;
- ◇ for the *Ankle* image the proposed CCGE–LS algorithm works better for each tested sampling pattern;
- ◇ the difference between the proposed CCGE–LS algorithm and its *Oracle* version is always unnoticeable for the radial and variable density patterns, but is more significant (about one order of magnitude) for the uniformly distributed sampling pattern. This means that in that case the initial gradient estimation the CCGE-LS algorithm relies on is less accurate and hence the bigger gap;
- ◇ finally, it can be noticed that the CoSaMP-CCGE–LS version of the proposed algorithm performs worse than the ℓ_1-CCGE–LS counterpart. This is probably due to the suboptimality of greedy algorithms like CoSaMP, which for such complex images tends to be significant and would require more iterations to obtain comparable performance.

V. Concluding Remarks

Since gradients of images are often much more sparse or compressible than the corresponding image, combination of CS algorithms and integration methods have been used for image recovery from spectral data. However these methods offer significant improvement in reconstruction quality and robustness over leading TV minimization only for high sampling ratio.

We have proposed new gradient based image recovery algorithms which combine constrained CS algorithms using curl information of gradient field with spectral graph filtering. Through extensive simulation, we have shown that the proposed algorithms outperform the state of the art also for small sampling ratio and for various sampling scenarios.

References

[1] M. Lustig, D. Donoho, and J. M. Pauly, "Sparse MRI: The application of compressed sensing for rapid MR imaging," *Magnetic Resonance in Medicine*, vol. 58, no. 6, pp. 1182–1195, 2007.

[2] V. M. Patel, G. R. Easley, D. M. Healy, and R. Chellappa, "Compressed sensing for synthetic aperture radar imaging," in *2009 16th IEEE International Conference on Image Processing (ICIP)*, Nov 2009, pp. 2141–2144.

[3] M. Lustig, D. L. Donoho, J. M. Santos, and J. M. Pauly, "Compressed sensing MRI," *Signal Processing Magazine, IEEE*, vol. 25, no. 2, pp. 72–82, 2008.

[4] E. J. Candes, J. Romberg, and T. Tao, "Robust uncertainty principles: exact signal reconstruction from highly incomplete frequency information," *IEEE Transactions on Information Theory*, vol. 52, no. 2, pp. 489–509, Feb 2006.

[5] E. J. Candes and J. Romberg, "ℓ_1-MAGIC," http://users.ece.gatech.edu/justin/l1magic/.

[6] J. M. Bioucas-Dias and M. A. Figueiredo, "TwIST: Two-step iterative shrinkage/thresholding algorithm for linear inverse problems," http://www.lx.it.pt/ bioucas/TwIST/TwIST.htm, 2007.

[7] ——, "A new TwIST: two-step iterative shrinkage/thresholding algorithms for image restoration," *Image Processing, IEEE Transactions on*, vol. 16, no. 12, pp. 2992–3004, 2007.

[8] S. Becker, J. Bobin, and E. J. Candès, "NESTA: a fast and accurate first-order method for sparse recovery," http://statweb.stanford.edu/ candes/nesta/, 2011.

TABLE I. MRI RECONSTRUCTION RELATIVE ERROR

Image	Sampling	GradientRec–Diff	RecPF	ℓ_1-CCGE–LS	Oracle	CoSaMP-CCGE–LS
Brain	Radial	3.32e-01	**7.90e-03**	4.07e-02	3.91e-02	1.33e-01
	Uniform	NaN	NaN	**1.38e-01**	1.38e-01	2.25e-01
	Variable Density	NaN	**6.66e-03**	7.42e-03	7.41e-03	1.31e-01
Knee	Radial	9.88e-02	4.36e-03	**3.86e-03**	3.85e-03	2.39e-01
	Uniform	5.74e-01	NaN	**2.11e-01**	4.79e-02	2.74e-01
	Variable Density	1.26e-01	**3.64e-03**	3.86e-03	1.74e-03	2.40e-01
Ankle	Radial	1.32e-01	3.73e-03	**3.67e-03**	1.39e-03	2.49e-01
	Uniform	5.51e-01	NaN	**2.07e-01**	1.24e-02	3.19e-01
	Variable Density	3.69e-02	2.78e-03	**2.39e-03**	1.02e-03	2.58e-01

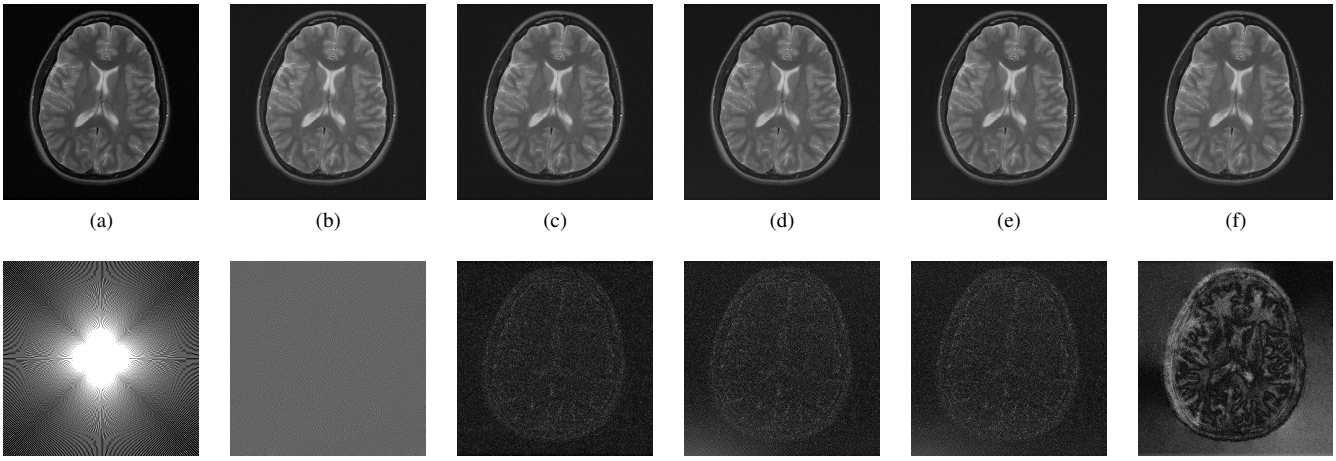

(a) (b) (c) (d) (e) (f)

(g) (h) (i) (j) (k) (l)

Fig. 9. Brain. Radial sampling. Compression Ratio $L = 0.4$. Top line: image reconstruction. Bottom line: error image. (a) Original. (g) Sampling pattern. (b) and (h) GradientRec–Diff. Relative Error: $3.32 \cdot 10^{-1}$. (c) and (i) RecPF. Relative Error: $7.90 \cdot 10^{-3}$. (d) and (j) ℓ_1-CCGE–LS. Relative Error: $4.07 \cdot 10^{-2}$. (e) and (k) Oracle. Relative Error: $3.91 \cdot 10^{-2}$. (f) and (l) CoSaMP-CCGE–LS. Relative Error: $1.33 \cdot 10^{-1}$.

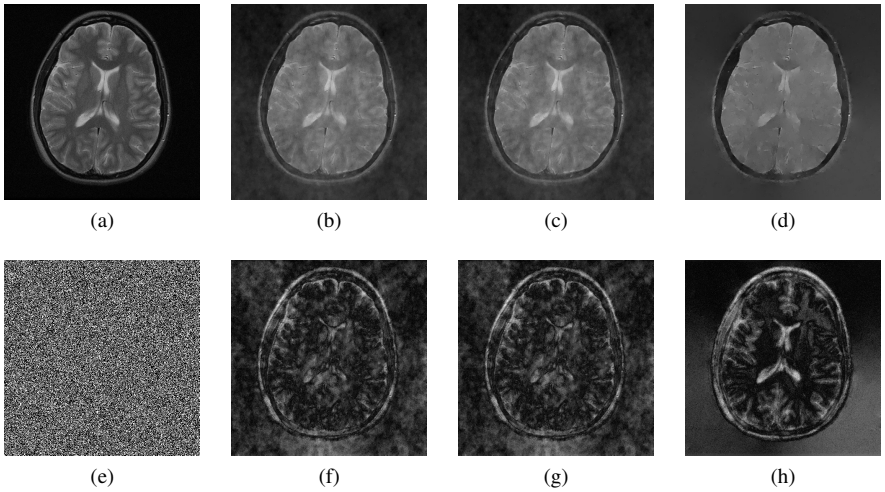

(a) (b) (c) (d)

(e) (f) (g) (h)

Fig. 10. Brain. Uniform sampling. Compression Ratio $L = 0.4$. Top line: image reconstruction. Bottom line: error image. (a) Original. (e) Sampling pattern. (b) and (f) ℓ_1-CCGE–LS. Relative Error: $1.38 \cdot 10^{-1}$. (c) and (g) Oracle. Relative Error: $1.38 \cdot 10^{-1}$. (d) and (h) CoSaMP-CCGE–LS. Relative Error: $2.25 \cdot 10^{-1}$. GradientRec–Diff and RecPF output a NaN.

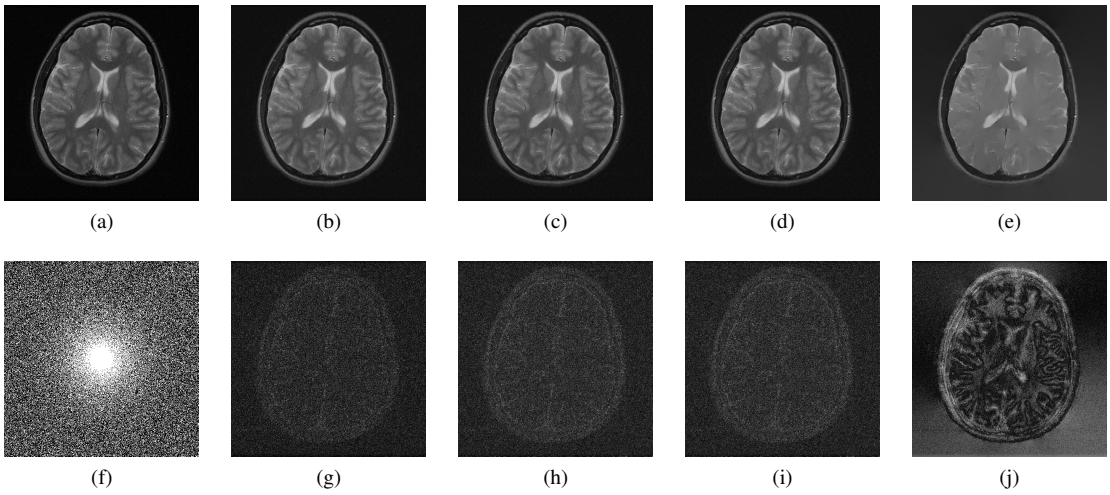

Fig. 11. Brain. Variable density sampling. Compression Ratio $L = 0.4$. Top line: image reconstruction. Bottom line: error image. (a) Original. (f) Sampling pattern. (b) and (g) RecPF. Relative Error: $6.66 \cdot 10^{-3}$. (c) and (h) ℓ_1-CCGE–LS. Relative Error: $7.42 \cdot 10^{-3}$. (d) and (i) Oracle. Relative Error: $7.41 \cdot 10^{-3}$. (e) and (j) CoSaMP-CCGE–LS. Relative Error: $1.31 \cdot 10^{-1}$. GradientRec–Diff output a NaN.

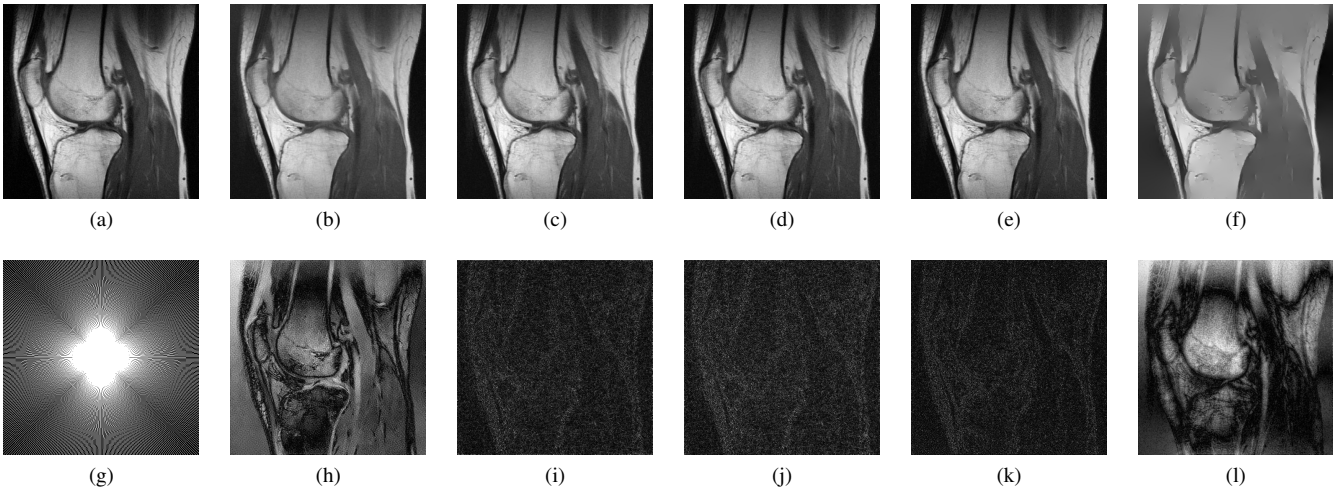

Fig. 12. Knee. Radial sampling. Compression Ratio $L = 0.4$. Top line: image reconstruction. Bottom line: error image. (a) Original. (g) Sampling pattern. (b) and (h) GradientRec–Diff. Relative Error: $9.88 \cdot 10^{-2}$. (c) and (i) RecPF. Relative Error: $4.36 \cdot 10^{-3}$. (d) and (j) ℓ_1-CCGE–LS. Relative Error: $3.86 \cdot 10^{-3}$. (e) and (k) Oracle. Relative Error: $3.85 \cdot 10^{-3}$. (f) and (l) CoSaMP-CCGE–LS. Relative Error: $2.39 \cdot 10^{-1}$.

[9] ——, "NESTA: a fast and accurate first-order method for sparse recovery," *SIAM Journal on Imaging Sciences*, vol. 4, no. 1, pp. 1–39, 2011.

[10] C. Li, W. Yin, and Y. Zhang, "TVAL3: TV minimization by Augmented Lagrangian and ALternating direction ALgorithms," http://www.caam.rice.edu/ optimization/L1/TVAL3/, 2009.

[11] ——, "User's guide for TVAL3: TV minimization by augmented lagrangian and alternating direction algorithms," *CAAM report*, vol. 20, pp. 46–47, 2009.

[12] J. Yang, Y. Zhang, and W. Yin, "A fast alternating direction method for TVL1-L2 signal reconstruction from partial Fourier data," *Selected Topics in Signal Processing, IEEE Journal of*, vol. 4, no. 2, pp. 288–297, 2010.

[13] V. M. Patel, R. Maleh, A. C. Gilbert, and R. Chellappa, "Gradient-based image recovery methods from incomplete fourier measurements," *Image Processing, IEEE Transactions on*, vol. 21, no. 1, pp. 94–105, 2012.

[14] S. Ma, W. Yin, Y. Zhang, and A. Chakraborty, "An efficient algorithm for compressed MR imaging using total variation and wavelets," in *Computer Vision and Pattern Recognition, 2008. CVPR 2008. IEEE Conference on*. IEEE, 2008, pp. 1–8.

[15] J. A. Tropp and A. C. Gilbert, "Signal recovery from random measurements via orthogonal matching pursuit," *Information Theory, IEEE Transactions on*, vol. 53, no. 12, pp. 4655–4666, 2007.

[16] D. Needell and J. A. Tropp, "CoSaMP: Iterative signal recovery from incomplete and inaccurate samples," *Applied and Computational Harmonic Analysis*, vol. 26, no. 3, pp. 301–321, 2009.

[17] I. Daubechies, R. DeVore, M. Fornasier, and C. S. Güntürk, "Iteratively reweighted least squares minimization for sparse recovery," *Communications on Pure and Applied Mathematics*, vol. 63, no. 1, pp. 1–38, Jan. 2010.

[18] E. J. Candès, M. B. Wakin, and S. P. Boyd, "Enhancing sparsity by reweighted ℓ_1 minimization," *Journal of Fourier Analysis and*

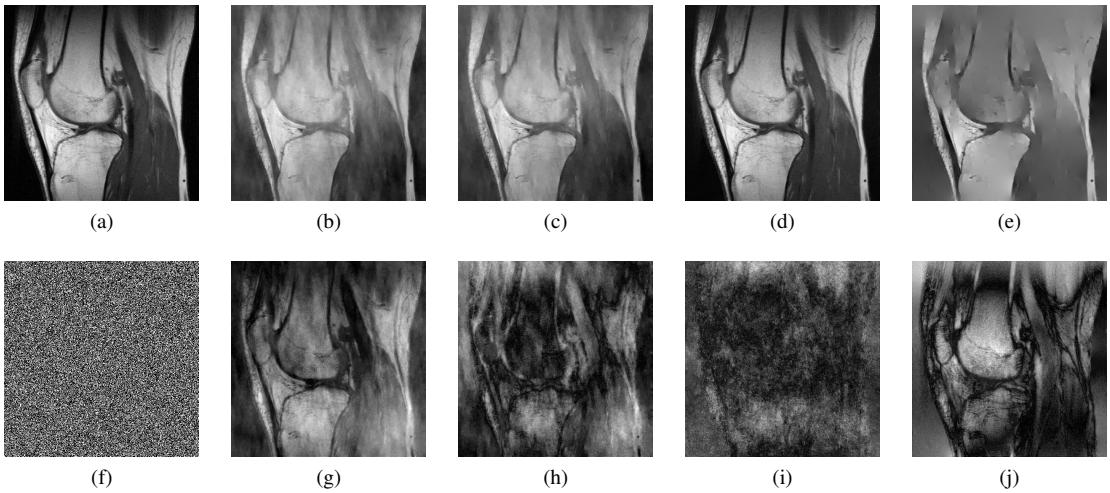

Fig. 13. Knee. Uniform sampling. Compression Ratio $L = 0.4$. Top line: image reconstruction. Bottom line: error image. (a) Original. (f) Sampling pattern. (b) and (g) GradientRec–Diff. Relative Error: $5.74 \cdot 10^{-1}$. (c) and (h) ℓ_1-CCGE–LS. Relative Error: $2.11 \cdot 10^{-1}$. (d) and (i) Oracle. Relative Error: $4.79 \cdot 10^{-2}$. (e) and (j) CoSaMP-CCGE–LS. Relative Error: $2.74 \cdot 10^{-1}$. RecPF output a NaN.

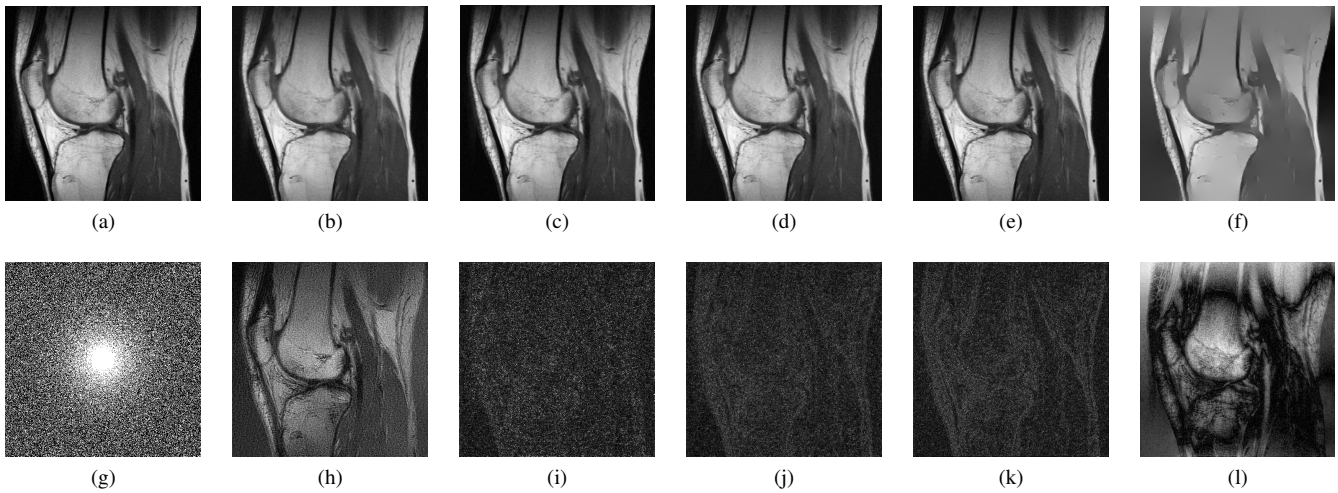

Fig. 14. Knee. Variable density sampling. Compression Ratio $L = 0.4$. Top line: image reconstruction. Bottom line: error image. (a) Original. (g) Sampling pattern. (b) and (h) GradientRec–Diff. Relative Error: $1.26 \cdot 10^{-1}$. (c) and (i) RecPF. Relative Error: $3.64 \cdot 10^{-3}$. (d) and (j) ℓ_1-CCGE–LS. Relative Error: $3.86 \cdot 10^{-3}$. (e) and (k) Oracle. Relative Error: $1.74 \cdot 10^{-3}$. (f) and (l) CoSaMP-CCGE–LS. Relative Error: $2.4 \cdot 10^{-1}$.

Applications, vol. 14, no. 5, pp. 877–905, 2008.

[19] A. Agrawal, R. Chellappa, and R. Raskar, "An algebraic approach to surface reconstruction from gradient fields," in *Tenth IEEE International Conference on Computer Vision (ICCV'05) Volume 1*, vol. 1, Oct 2005, pp. 174–181 Vol. 1.

[20] A. Agrawal, R. Raskar, and R. Chellappa, "What is the range of surface reconstructions from a gradient field?" in *Proceedings of the 9th European Conference on Computer Vision - Volume Part I*, ser. ECCV'06. Berlin, Heidelberg: Springer-Verlag, 2006, pp. 578–591.

[21] E. van den Berg and M. P. Friedlander, "SPGL1: A solver for large-scale sparse reconstruction," http://www.cs.ubc.ca/labs/scl/spgl1, June 2007.

[22] ——, "Probing the Pareto frontier for basis pursuit solutions," *SIAM Journal on Scientific Computing*, vol. 31, no. 2, pp. 890–912, 2008. [Online]. Available: http://link.aip.org/link/?SCE/31/890

[23] D. I Shuman, S. K. Narang, P. Frossard, A. Ortega, and P. Vandergheynst, "The emerging field of signal processing on graphs: Extending high-dimensional data analysis to networks and other irregular domains," *IEEE Signal Processing Magazine*, vol. 30, no. 3, pp. 83–98, May 2013.

[24] P. Barooah and J. P. Hespanha, "Error scaling laws for linear optimal estimation from relative measurements," *Information Theory, IEEE Transactions on*, vol. 55, no. 12, pp. 5661–5673, 2009.

[25] G. Strang, "The discrete cosine transform," *SIAM Review*, vol. 41, no. 1, pp. 135–147, 1999.

[26] V. M. Patel, G. R. Easley, R. Chellappa, and D. M. Healy Jr, "Enhancing sparsity using gradients for compressive sensing," in *Image Processing (ICIP), 2009 16th IEEE International Conference on*. IEEE, 2009, pp. 3033–3036.

[27] F. Krahmer and R. Ward, "Stable and robust sampling strategies for compressive imaging," *Image Processing, IEEE Transactions on*, vol. 23, no. 2, pp. 612–622, 2014.

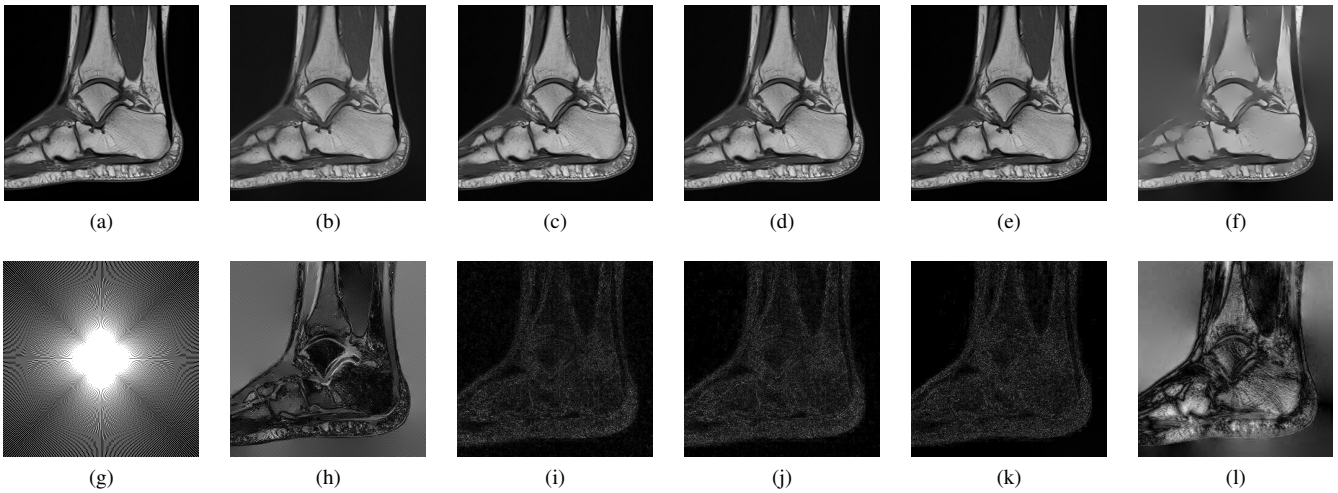

Fig. 15. Ankle. Radial sampling. Compression Ratio $L = 0.4$. Top line: image reconstruction. Bottom line: error image. (a) Original. (g) Sampling pattern. (b) and (h) GradientRec–Diff. Relative Error: $1.32 \cdot 10^{-2}$. (c) and (i) RecPF. Relative Error: $3.73 \cdot 10^{-3}$. (d) and (j) ℓ_1-CCGE–LS. Relative Error: $3.67 \cdot 10^{-3}$. (e) and (k) Oracle. Relative Error: $1.39 \cdot 10^{-3}$. (f) and (l) CoSaMP-CCGE–LS. Relative Error: $2.49 \cdot 10^{-1}$.

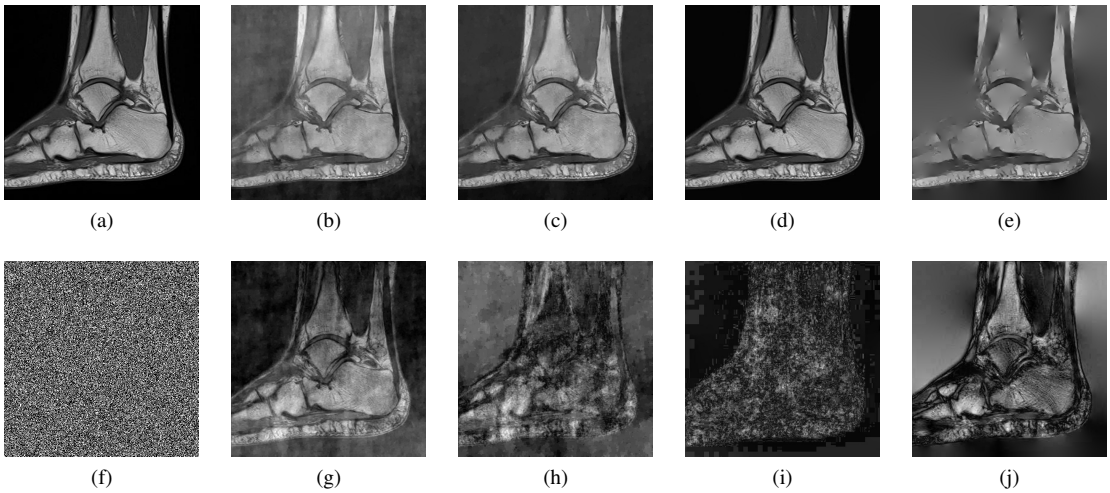

Fig. 16. Ankle. Uniform sampling. Compression Ratio $L = 0.4$. Top line: image reconstruction. Bottom line: error image. (a) Original. (f) Sampling pattern. (b) and (g) GradientRec–Diff. Relative Error: $5.51 \cdot 10^{-1}$. (c) and (h) ℓ_1-CCGE–LS. Relative Error: $2.07 \cdot 10^{-1}$. (d) and (i) Oracle. Relative Error: $1.24 \cdot 10^{-2}$. (e) and (j) CoSaMP-CCGE–LS. Relative Error: $3.19 \cdot 10^{-1}$. RecPF output a NaN.

Chiara Ravazzi Chiara Ravazzi (M'13) received the B.Sc. and M.Sc., and Ph.D. degrees in applied mathematics from Politecnico di Torino, Italy, in 2005 and 2007, and 2011 respectively. During 2010, she was a visiting member at the Laboratory for Information and Decision Systems, Massachusetts Institute of Technology, Cambridge. From 2011 to 2012 she was a research assistant at the Department of Mathematics of Politecnico di Torino. From 2012 to 2016, she was a Post-Doc at the Department of Electronics and Telecommunications of Politecnico di Torino, developing algorithms for sparse recovery problems, within the project "Towards compressive information processing systems" funded by the European Union as ERC starting grant (2012 - 2016) under the supervision of Prof. Enrico Magli. From 2013 to 2016, she has been a Research associate at the Institute of Electronics, Computer and Telecommunication Engineering (IEIIT) of the National Research Council of Italy (CNR). Since 2017, she is a Tenured Researcher of the National Research Council of Italy (CNR) at the Institute CNR-IEIIT, working in the Systems & Control Technologies (SCT) Group.

She is author of more than 30 works published in international journals, books, and proceedings of international conferences. Her current research interests lie in the broad areas of signal processing, optimization and learning algorithms for intelligent networked systems. Example projects include: compressive sensing and optimization for signal and image recovery; distributed compressed sensing, distributed optimization, control and optimization of dynamics over networks.

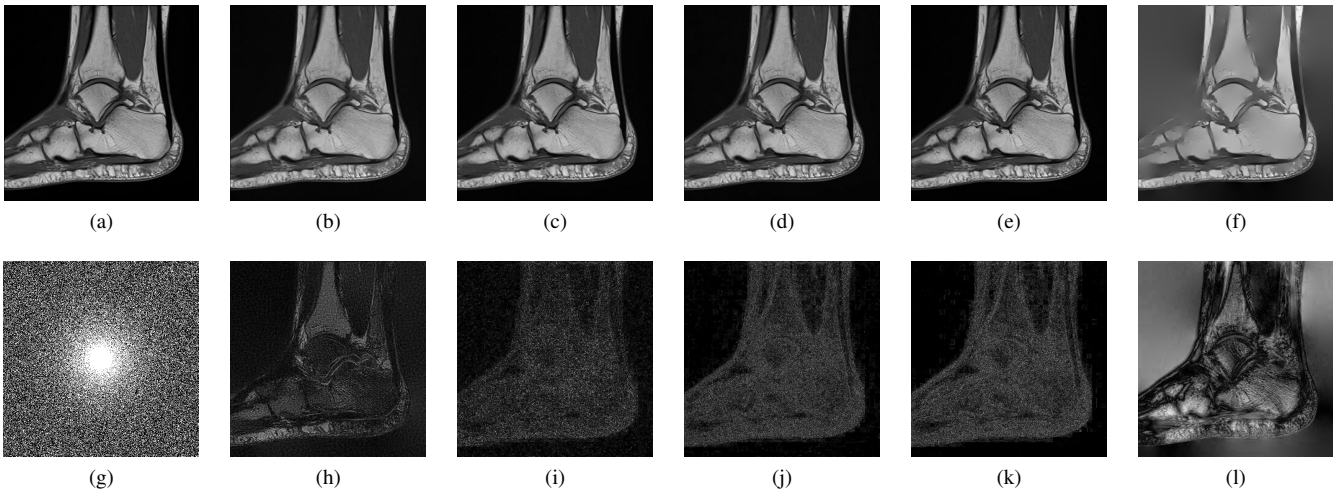

(a) (b) (c) (d) (e) (f)

(g) (h) (i) (j) (k) (l)

Fig. 17. Ankle. Variable density sampling. Compression Ratio $L = 0.4$. Top line: image reconstruction. Bottom line: error image. (a) Original. (g) Sampling pattern. (b) and (h) GradientRec–Diff. Relative Error: $3.69 \cdot 10^{-2}$. (c) and (i) RecPF. Relative Error: $2.78 \cdot 10^{-3}$. (d) and (j) ℓ_1-CCGE–LS. Relative Error: $2.39 \cdot 10^{-3}$. (e) and (k) Oracle. Relative Error: $1.02 \cdot 10^{-3}$. (f) and (l) CoSaMP-CCGE–LS. Relative Error: $2.58 \cdot 10^{-1}$.

Giulio Coluccia Giulio Coluccia (M'12) received the B.Sc. in 2003 and the M.Sc. in 2005 in Telecommunications Engineering, both from the Politecnico di Torino, Torino, Italy. He received the Ph.D. degree in Electronic and Communications engineering in 2009 from the Electronics Department of the Politecnico di Torino, Torino, Italy, under the supervision of prof. Giorgio Taricco.

Currently, he is a Post Doctoral Researcher within the Image Processing Lab at Politecnico di Torino, leaded by Prof. Enrico Magli. His resarch is focused on Compressed Sensing, with particular interest in its application to Image Processing and Forensics, Multidimensional Signals and to Distributed Source Coding and Wireless Sensor Networks. He is involved in the 5-year ERC project entitled "CRISP - Towards compressive information processing systems" funded by the European Research Council.

Enrico Magli Enrico Magli (S'97 - M'01 - SM'07 - F'17) received the M.Sc. and Ph.D. degrees from the Politecnico di Torino, Torino, Italy, in 1997 and 2001, respectively. He is currently an Associate Professor with Politecnico di Torino, Torino, Italy. His research interests include compressive sensing, image and video coding, and vision. He is an Associate Editor of the IEEE TRANSACTIONS ON MULTIMEDIA and the EURASIP Journal on Image and Video Processing, and a former Associate Editor of the IEEE TRANSACTIONS ON CIRCUITS AND SYSTEMS FOR VIDEO TECHNOLOGY. He is a Fellow of the IEEE, and has been an IEEE Distinguished Lecturer from 2015 to 2016. He was the recipient of the IEEE Geoscience and Remote Sensing Society 2011 Transactions Prize Paper Award, the IEEE ICIP 2015 Best Student Paper Award (as senior author), and the 2010 and 2014 Best Associate Editor Award of the IEEE TRANSACTIONS ON CIRCUITS AND SYSTEMS FOR VIDEO TECHNOLOGY.